

Submicrosecond Field-Jump Device for Pulsed High-Field ELDOR

A. A. Dubinskii¹, Yu. A. Grishin², A. N. Savitsky³, and K. Möbius³

¹Semenov Institute of Chemical Physics, Russian Academy of Sciences,
Moscow, Russian Federation

²Institute of Chemical Kinetics and Combustion, Russian Academy of Sciences,
Novosibirsk, Russian Federation

³Institute of Experimental Physics, Free University Berlin, Berlin, Germany

Received January 16, 2002

Abstract. A field-jump device for fast stepping the electron paramagnetic resonance magnetic field around 3.4 T during pulsed electron-electron double resonance experiments at W-band (95 GHz) is described. Field jumps up to ± 160 G and submicrosecond times for the full field-jump cycle allow precession frequency transfer experiments to be made for the determination of the nanometer distance and the orientation of nitroxide spin-label pairs in disordered samples.

1 Introduction

Modern electron paramagnetic resonance (EPR) spectroscopy is distinguished by three important developments: pulsed microwave techniques, double-resonance techniques, and high-Zeeman-field techniques. EPR becomes particularly powerful when these techniques are combined in the same experiment. Thus, electron-electron double resonance performed in pulsed mode, known as PELDOR or DEER, is very powerful for measuring weak spin-spin interactions between remote paramagnetic centers in disordered solids [1–3]. A broad avenue for applications of this methodology to investigate the structure of large biological systems is opened by the recent progress in site-directed spin labeling [4, 5]. After selectively introducing spin labels into certain pairs of structural segments, one can probe the distance between and the orientation of these segments via the dipole-dipole interaction within such pairs of spin labels [3, 6, 7]. Orientational information in disordered solids is, of course, available only at a sufficient degree of orientation selectivity in the spin-label spectrum. Therefore, performing PELDOR experiments in high-field EPR, where the Zeeman selectivity increases considerably [8], looks like a promising improvement of this technique. In the present work, we consider technical possibilities to perform pulsed double electron-electron resonance spectroscopy, thereby resolving weak dipole-dipole interactions at high magnetic fields.

A complete PELDOR study requires resonant microwave pulses to be applied sequentially at different spectral positions and to be swept over the full frequency range of the EPR spectrum of the paired radicals. Obviously, this requirement creates bandwidth problems with high-quality factor (Q) microwave cavities of the EPR spectrometer if the EPR spectrum covers a broad spectral region. In this work we describe different PELDOR strategies, dual-frequency PELDOR at fixed magnetic field and field-jump PELDOR at fixed microwave frequency, with regard to their ability to satisfy the requirements of broad spectral coverage at high Zeeman field. Here, the first realization of a fast field-jump device for W-band (95 GHz) EPR is reported which allows one to change resonance conditions by field jumps of amplitudes up to ± 160 G within submicrosecond time intervals. Such characteristics are essential for pulsed dipole-resolving W-band EPR spectroscopy of spin-labeled biosystems.

2 Pulsed High-Field ELDOR: Dual-Frequency or Field-Jump Technique?

Because of the broad microwave frequency range typical for nitroxide radical EPR spectra, PELDOR is restricted by selective excitation, i.e., the pulses applied can excite only a small part of the spectrum. Two strategies can be used for sequential pulse excitation of different spectral parts. (Actually, one more type of pulsed dipolar EPR spectroscopy was reported recently [9] which operates with multiple nonselective microwave pulses. In this mode of operation one excites the complete spectral range, if possible, or at least certain isotropic and well-separated spectral components, if present. This results in a dipolar frequency spectrum summed over randomly oriented spin pairs in disordered solids, i.e., the Pake pattern. From this pattern, one can directly read off the splitting related to the

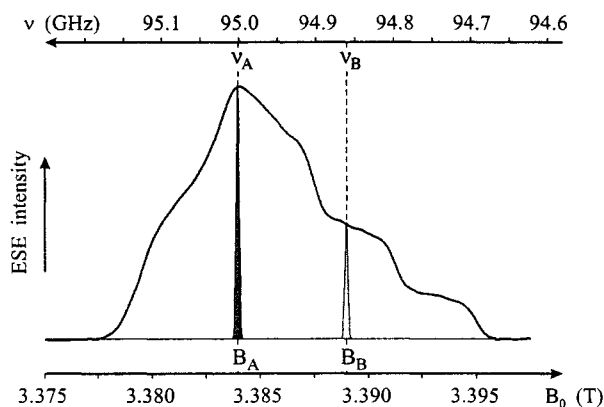


Fig. 1. Echo-detected W-band EPR spectrum of ^{14}N nitroxide radicals in disordered solids. Lower and upper scales give the field- and frequency-domain representation of the spectrum, respectively. B_A and B_B fields (ν_A and ν_B frequencies) denote the resonance positions of the A spins and B spins, selected for PELDOR measurements according to the pulse schemes shown in Fig. 2.

intra-pair distance. The orientational information, however, is completely skipped. This novel technique, operating with a single microwave frequency at fixed field, is not further included in our discussion.)

The first strategy for pulsed ELDOR is dual-frequency PELDOR (DF-PELDOR) [10–12], where the measurements are made at a fixed magnetic field value B_0 with two microwave (mw) sources. They are tuned to frequencies corresponding to the spectral positions selected for observing (spins A, ν_A) and for pumping (spins B, ν_B), see Fig. 1. For the dipole-resolving spectroscopy, the pulse pattern for the A spins is an echo-forming train (for example, the primary echo sequence $\pi/2$ – τ – π – τ –signal), while the B spins are flipped at an instant between the first pulse of the A train and its echo signal by an additional π pulse at ν_B , as is shown in Fig. 2a.

The second strategy for pulsed ELDOR is to select the pairs of double-resonance positions rather by a magnetic field offset, ΔB , than by a second mw frequency. In this case, a single mw source is used tuned to the cavity frequency ν_0 , corresponding to ν_A at B_A . The magnetic field is stepped rapidly from one position (B_A) within the EPR spectrum to another position ($B_B = B_A + \Delta B$) right after the first two mw $\pi/2$ -pulses, and then returned quickly back to B_A during the precession-free period T of the stimulated-echo sequence, as is shown in Fig. 2b [13–16]. We call this technique field-jump PELDOR (FJ-PELDOR).

To compare these two techniques, we first outline the principles of dipolar PELDOR spectroscopy on the basis of the simple magnetization vector model shown in Fig. 3. Here we consider the dipole interaction in terms of the dipole magnetic field, B_d , induced on the radical A by the magnetic moment of the spin

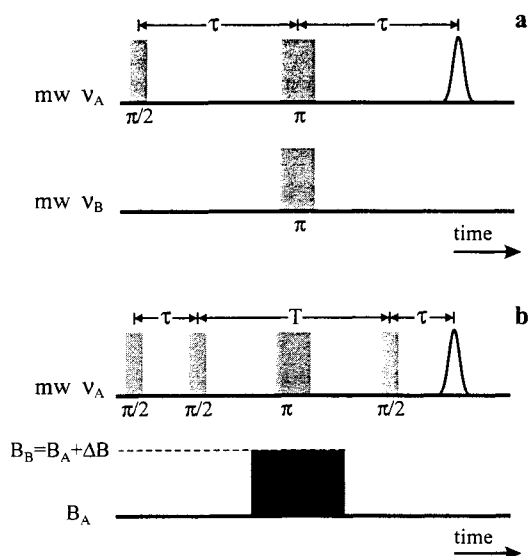


Fig. 2. Pulse patterns for DF-PELDOR (a) and FJ-PELDOR (b) experiments. The mw frequencies ν_A and ν_B , as well as the fields B_A and $B_B = B_A + \Delta B$, correspond to those of Fig. 1.

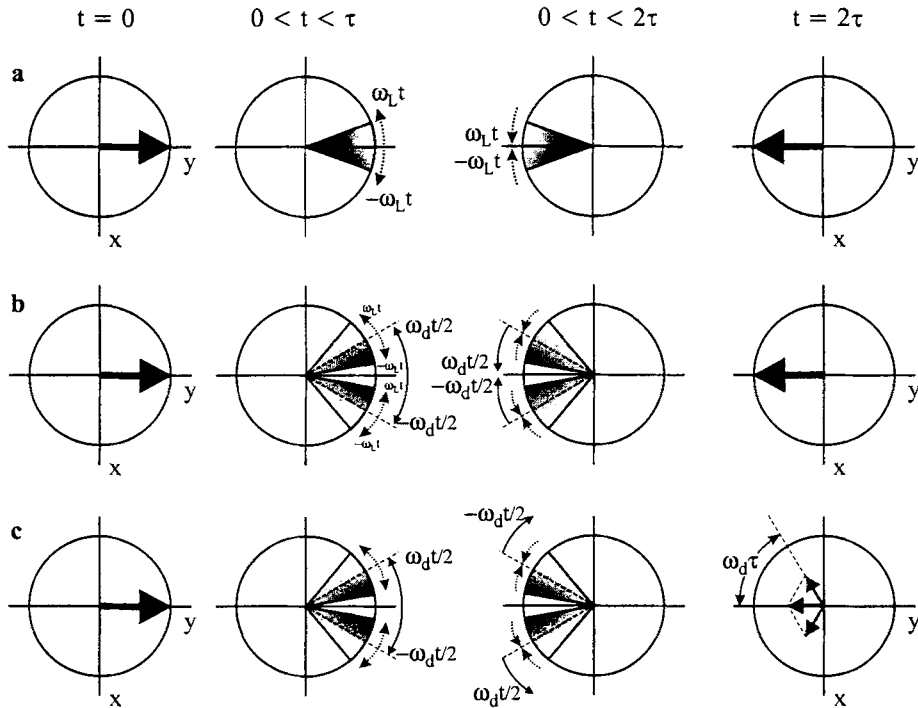


Fig. 3. Transversal-magnetization behavior in ω_A -rotating frame ($\omega = 2\pi\nu$) following an echo-forming ($\pi/2-\tau-\pi$) pulse sequence. **a** Spins A without a dipolar coupling to spins B. During evolution time the subensemble magnetization vectors rotate with slightly different angular velocities, ω_L , due to different local fields they experience. **b** Spins A with a dipolar coupling to spins B, for the definition of ω_d , see Eq. (1). **c** Spins A with a dipolar coupling to spins B, but now applying an additional π pulse that flips spins B, see Fig. 2a. In some of the diagrams in **b** and **c** the marking of the dephasing rate, $\omega_L t$, has been omitted for clarity.

B (and vice versa). This approximation holds under the condition $|B_d| \ll |B_A - B_B|$, which can be assumed for large interspin distances and small dipolar couplings measured by the PELDOR method. The field B_d , adding to the external field B_0 , shifts the resonance frequency of the A spins for $\pm \nu_d/2$, where the positive or negative sign of the shift depends on the α or β state of the inducing spin, and ν_d is determined by:

$$h\nu_d = \mu_0 \frac{\beta^2 g_A g_B}{r_{AB}^3} (3 \cos^2 \theta_{AB} - 1), \quad (1)$$

where μ_0 is the vacuum permeability, β is the Bohr magneton, g_A and g_B are effective g factors of the respective radicals (principal components of the g -tensors weighed according to their orientation in the pair), r_{AB} is the intra-pair distance, and θ_{AB} is the angle between the pair director and the spectrometer mag-

netic field B_0 . These frequency shifts result in additional precession-phase angles, $\pm \omega_d \tau / 2$ ($\omega_d = 2\pi \nu_d$), accumulated during the first τ period of the echo sequence, as shown in Fig. 3b. If the dipole field does not change until the echo-detection time 2τ , the dipolar dephasing will become compensated (together with other stationary local offsets ω_L shown in Fig. 3a) after the second τ period following the π pulse (that inverts transversal magnetization along the y -axis). However, if the B spins had been flipped before the refocusing started, their dipole fields at the A spins become inverted. Then the further precession of the A spins occurs with correspondingly modified frequency, as shown in Fig. 3c. Instantaneous transfer of precession frequency results in a specific modulation of the following echo signal and, therefore, the dipole-interaction frequency ν_d can be extracted by Fourier analysis of this modulation [10].

Although DF-PELDOR is technically much better developed than FJ-PELDOR, its actual realization still encounters serious problems because of the limited bandwidth of the EPR cavity, $\Delta\nu = \nu_0/Q$. Indeed, for pulsed X-band EPR with $\nu_0 \approx 10$ GHz and $Q \approx 300$, the mw irradiation amplitude strongly decreases for frequency offsets $|\nu - \nu_0| > 30$ MHz. This bandwidth is narrower than the frequency range of most EPR spectra of interest, including that of nitroxide spin labels (about 200 MHz). Therefore, it does not allow dual irradiation with properly separated mw frequencies. Some increase of bandwidth can, of course, be achieved by further lowering Q , thereby sacrificing, however, detection sensitivity. Actually, to allow for fast mw pulsing and signal processing, pulsed X-band EPR normally operates at Q values of several hundreds, which are already reduced as compared to those of several thousands used for continuous-wave (cw) EPR. For PELDOR experiments Q must be lowered even more, which results in a decrease of a signal-to-noise ratio and a decrease of the mw field amplitude, B_1 , at the sample. To perform DF-PELDOR experiments without substantial loss of these quantities, special bimodal cavities can be used [17, 18]. However, a proper frequency sweep turned out to be rather problematic in these cavities. Another approach is to use special broad-band resonance structures with increased B_1 density at the sample, such as loop-gap resonators [19] or resonators with mw field concentrating inserts [20]. Unfortunately, these structures become rather miniature even at X-band, and they certainly become too small for manufacturing and operating at W-band. On the other hand, considerable increase of bandwidth, even for a single-mode cavity with high Q , can be achieved in high-field and high-frequency EPR because of the increased ν_0 : for $\nu_0 = 100$ GHz (W-band) and $Q = 1000$, the bandwidth equals 100 MHz. Note that this bandwidth already allows for fast pulsing and signal processing. However, also the spectral width of the radicals expands in high-field EPR as compared to X-band EPR: W-band EPR spectra of nitroxide radicals are spread over a range of 400 MHz as compared to 200 MHz at X-band. Therefore, the bandwidth advantage of high-field EPR is still not sufficient for DF-PELDOR of nitroxides, and consequently, we consider the field-jump alternative of PELDOR as an adequate solution to the problem.

Rapid field-stepping and field-gradient devices for pulsed EPR have been designed earlier [13, 16, 21, 22]. The main difference of the present device is its application to high-field EPR (W-band) and its accommodation to the specific requirements of dipole-resolving PELDOR. These requirements are as follows.

1. Field amplitude, ΔB . It should be large enough to allow both resonance fields, B_A and B_B , to be positioned at any value within the nitroxide W-band EPR spectrum, i.e., at least ± 150 G.

2. Drift of the stepped field, $d\Delta B/dt$. After being generated, the field ΔB should be stable enough to prevent a drift from the B_B resonance position during the time τ_π when the microwave π pulse flips the B spins. We assume this drift to be negligible if $(d\Delta B/dt)t_\pi < B_1$ holds, where B_1 is the amplitude of the mw pulse. For the typical case of $t_\pi = 0.2 \mu\text{s}$ at $B_1 = 0.8$ G, this results in $(d\Delta B/dt) < 4$ G/ μs . A technically possible increase of B_1 with according reduction of t_π makes this requirement even less critical.

3. Residual field amplitude, B_{off} . Inasmuch as the stepped field ΔB cannot be switched off instantaneously, some residual field is present long after the field-inducing current is switched off. To minimize the effect of this field on the echo signal, its amplitude after the last $\pi/2$ pulse should satisfy the condition $\gamma\Delta B_{\text{off}}\tau \ll 1$. Measurements for resolving small dipole splittings require long-ranged sweeps of τ , the time between first two $\pi/2$ pulses. Therefore, this requirement can be rather critical.

4. Field-pulse length, t_{fp} . This time interval is counted from the instant at which the stepped field at the sample starts to change, includes the time required to reach the stationary field amplitude (t_{on}), the time to execute the π pulse (t_π , see requirement 2) and, additionally, the time required to switch the field off (t_{off}), i.e., the time until the residual field has decayed to the acceptable value discussed above. The complete field excursion is enclosed within the time interval of the stimulated-echo sequence (T , see Fig. 2). This has to be short enough to avoid relaxation losses of the echo signal. For nitroxide radicals at properly low temperature (below about 120 K) the echo-decay constant exceeds 10 μs , and thus, an estimated t_{fp} of a few microseconds appears appropriate. However, as is shown in this work (see below), the transient eddy currents, induced in the spectrometer probehead by field-stepping, create considerable and long-lasting shielding fields which expand t_{on} and t_{off} much over a microsecond scale. To make these transient fields smaller or their decay faster, certain modifications in the probehead construction are required. Because the eddy fields created by the on- and off-steps of the external field are oppositely directed, they subtract after the jump cycle. This results in a reduction of the residual field: the shorter the external field pulse is, the more complete is the subtraction. Therefore, the field-pulsing device should operate in a submicrosecond time scale.

5. Field inhomogeneity, $\Delta\Delta B$. Any inhomogeneity of the stepped field ΔB across the sample will affect the flip angle of the B spins (deviations from π) and broaden their excitation range. To minimize these effects, the condition $\Delta\Delta B < B_1$ should be fulfilled. For the inhomogeneity of the residual field, $\Delta\Delta B_{\text{off}}$, which will reduce the echo signal, the corresponding condition is $\gamma\Delta\Delta B_{\text{off}}\tau \ll 1$.

Our preliminary considerations had shown that the construction of a field-jump device that satisfies all the requirements above is a technically challenging task. The main problem is that the fast-stepped field generates eddy currents in the conductive parts of the probehead (cavity walls, coupling waveguide, etc.), which, in high-field and high-frequency EPR, are in close proximity of the sample. The eddy currents, in turn, induce transient reaction fields superimposing with the applied stepped field. This effect is well known, of course, and results, for example, in a partial shielding of alternating radio-frequency fields applied for Zeeman modulation in cw EPR or electron-nuclear-double-resonance (ENDOR) experiments. Amplitude and time characteristics of these reactive magnetic fields, generated by pulsed eddy currents, are difficult to predict theoretically but may be rather evaluated experimentally. Another open question, which had to be clarified experimentally, is the magnitude of echo-signal distortions that are caused by the field-jump procedure via electromagnetic (rapidly changing high currents and voltages) and/or mechanical (strong current pulses within the B_0 field create shock waves) pathways. In Sects. 3–5 we describe the field-jump device designed for FJ-PELDOR experiments in W-band high-field EPR and report the results of its experimental test.

3 Construction of the Field-Jump Device

The pulsed magnetic field at the sample inside the W-band EPR cavity was generated by a pulsed current through a pair of Helmholtz coils fixed outside the cavity (Fig. 4b). Each coil consists of 3 turns of insulated copper wire (diameter of 0.8 mm) wound around a cylindrical holder (diameter of 22 mm). The separation between the coils equals 11 mm. The coils are electrically connected in series, and the measured inductance, $L = 0.9 \mu\text{H}$, agrees with that calculated for the coil geometry. The calculated field homogeneity over a typical sample dimension (below 1 mm) is better than 0.3% of the generated field amplitude. The calculated field-current conversion coefficient is 2.37 G/A. Thus, for the maximum field of 160 G, a pulsed current of 70 A is required. The general design and coil dimensions were adapted to the laboratory-built W-band EPR spectrometer described elsewhere [23].

The pulsed current generator shown in Fig. 4a is based on two commercial electronic devices.

1. The high-voltage DC source (HCE 35-2000; F. u. G. Elektronik, Rosenheim, Germany) supplies a stabilized voltage from 0 to 2000 V with 10^{-4} precision and a maximum output current of 15 mA.

2. The fast high-voltage FET semiconductor switch (HTS 51-20; Behlke Electronic, Kronberg, Germany) with the following specified characteristics: 5000 VDC/200 A; turn-on rise time, 35 ns; turn-off fall time, 30 ns; minimum pulse duration, 200 ns. An optical isolator (HP2601 + SN74126; Hewlett Packard, Palo Alto, USA) between the external trigger source and the FET switch was used in order to avoid galvanic coupling and to reduce propagation of noise spikes over the connecting line that are created by the pulsed current.

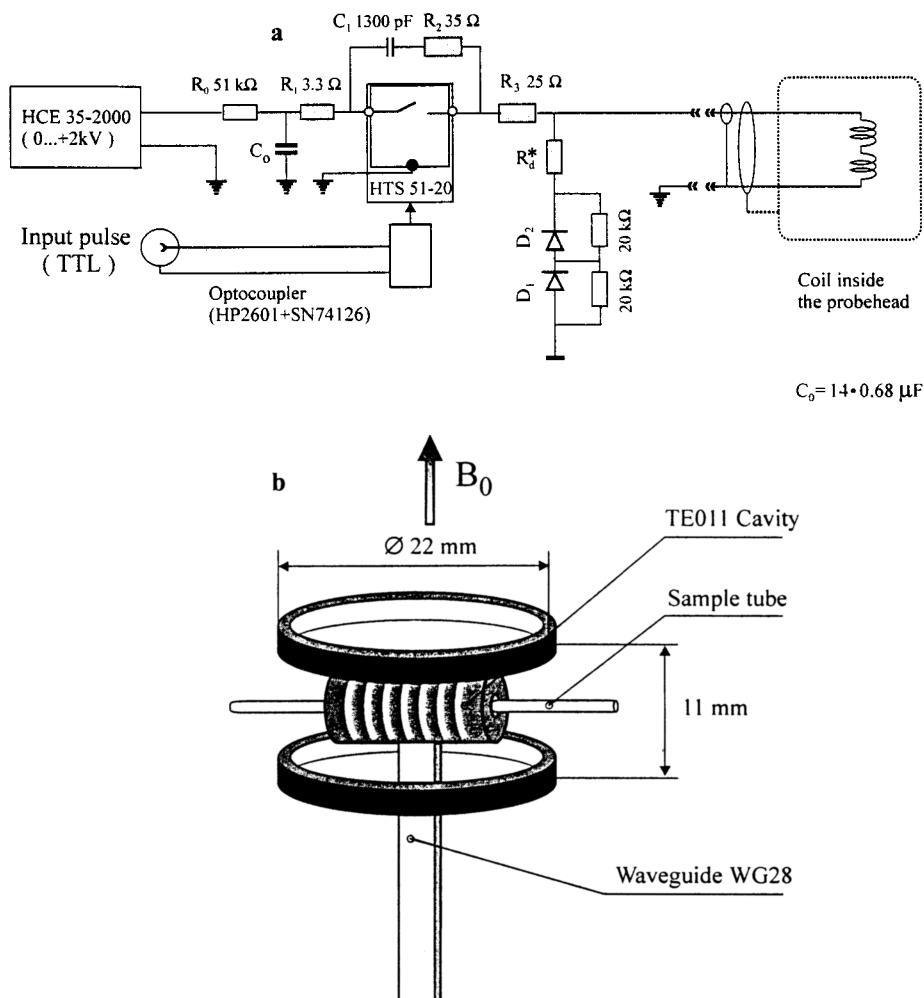


Fig. 4. a Basic electric scheme of the current-stepping device; b probehead with the Helmholtz coils and slotted W-band cavity. For details, see text.

The DC source of controlled voltage U_0 charges capacitor C_0 (14 by 0.68 mF high-voltage capacitors; WIMA, Mannheim, Germany) through resistor R_0 . The charged capacitor is then periodically discharged through the loading circuit with the coil inside the probehead by short current pulses gated with the fast FET switch. If we assume for a moment a completely resistive load ($R_1 + R_3 \approx R_3$), discharge occurs exponentially with time constant $\tau_1 = R_3 C_0$. For a short gating period, $t_p \ll \tau_1$, the pulsed current has a quasi-rectangular time profile with a plane top and transient on- and off-pulse behavior determined by the switch. The amplitude of this current, $I_p = U_c / R_3$, is controlled by the ca-

pacitor voltage $U_c = U_0[1 - \exp(-T/\tau_0)][1 - \exp(-t_p/\tau_0)\exp(-T/\tau_0)]^{-1}$, where $\tau_0 = R_0C_0$ and T is the pulse repetition period. For $R_3 \ll R_0$, this current can be made much larger than the maximum current allowed for the DC source. Thus, for $U_0 = 2000$ V and $R_3 = 25 \Omega$, the pulsed current I_p reaches 80 A, in accordance with our requirements.

Because the actual load of the DC source includes the inductance, L , of the coils the stepped current approaches its maximum value exponentially with time constant $t_L = L/R_{id}$, where $R_{id} = R_1 + R_3 + R_L \approx R_3$. Therefore, the current-control resistor $R_3 = 25 \Omega$ is chosen as to satisfy both requirements, strong peak current and short time constant. The power return pathway through the two fast-recovery diodes D_1 and D_2 (BY329-1200; Philips Semiconductors, Eindhoven, Netherlands; 65 A, 1200 V, 145 ns) and bulk resistor R_d^* was installed for improvement of the trailing edge of the current pulse. To minimize ringings and oscillations following the current on- and off-switching, the correction circuit C_1 - R_2 was introduced according to recommendations of the FET-switch producer (Behlke Electronic).

The pulsed current-generator unit was positioned at minimum distance (about 60 cm) from the EPR probehead to minimize the length of the transmission cable and to reduce distortions of the pulse shape by cable capacitance and line mismatch. The stray field of the spectrometer magnet at this place is about 500 G. To prevent possible influences of this field on the FET switch, it was installed within a screening μ -metal box. The coaxial cable (RG-3) has additional copper shielding connected to the probehead, as shown in Fig. 4a.

4 Tests of the Field-Jump Device

4.1 Current Measurements

Representative coil-current time profiles measured with a P6019 AC Current Probe (Tektronix, Beaverton, USA) are shown in Fig. 5a. Their analysis reveals the following characteristics. The turn-on delay time, determined by the high-voltage FET switch, is 175 ns, independent of the voltage setting; the current-pulse duration, measured for trigger pulses from 200 ns to 5 μ s, equals the trigger-pulse length plus 110 ns; this extension, caused by the FET switch and correction circuits, is almost independent of the pulse length; the rise-time profile is well described by a single exponential with 44 ± 2 ns time constant. It is independent of voltage and pulse length, and 99% of the maximum current is reached in about 200 ns, the fall-time profile is, to a good approximation, single-exponential with 25 ± 2 ns time constant, and 1% of the maximum current is reached in about 125 ns; the relative amplitudes of current pulses correspond to the voltage settings.

The measured current profiles reproduce the time behavior of the magnetic field generated by the stand-alone coils, i.e., without EPR probehead. However, in the FJ-PELDOR experimental setup this coil-generated magnetic field superimposes, at the sample position, with the reactive magnetic field of the eddy currents induced in the EPR cavity walls and the other conductive parts of the

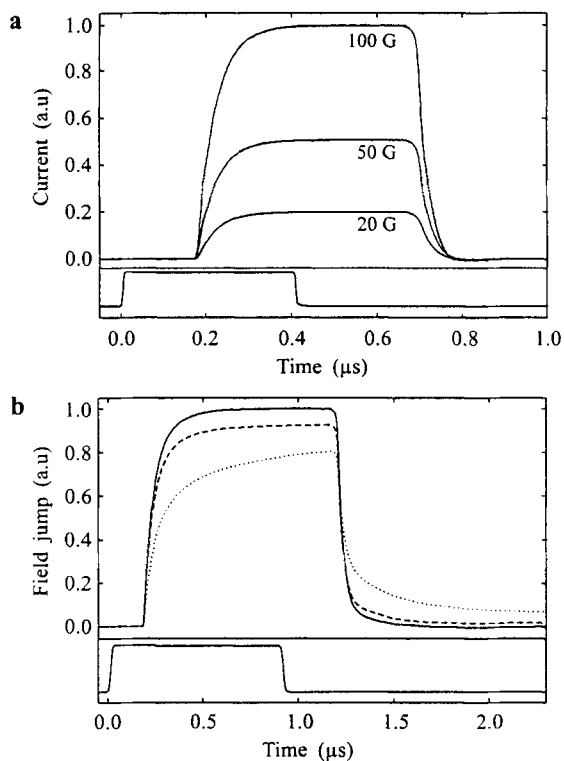


Fig. 5. **a** Representative coil-current time profiles taken for a trigger pulse of 400 ns (shown below) at field-jump amplitudes of 20, 50 and 100 G. **b** Time profiles of the magnetic field jump obtained by the pick-up coil for a 100 G, 1 μ s jump: solid line, stand-alone jump coils; dashed line, jump coils mounted on the probehead without EPR cavity; dotted line, jump coils mounted on the probehead with slotted brass cavity. The lower trace shows a trigger pulse of 900 ns.

probehead. To reduce this reactive field, we used the gold-plated brass TE_{011} cylindrical cavity with partially slotted walls that was designed earlier [23] for ENDOR experiments (the slots are indicated in Fig. 4b). At this stage of our investigation no additional changes of this ENDOR probehead were done to further reduce eddy currents. Actually, we wanted to base the construction of an optimized field-jump probehead on the experimental evaluation of the eddy-field effects in the brass cavity. Considerable contributions of the reactive field to the actual magnetic field at the sample position were traced by direct field measurements.

4.2 Magnetic-Field Measurements

A small pick-up coil (Cu of diameter of 0.2 mm, 5 turns, diameter of ca. 1 mm, length of ca. 1 mm) was used to measure the pulsed-field characteristics.

The field profiles, $\Delta B(t)$, were obtained by numerical integration, $\Delta B(t) \propto \int V(t)dt$, of the measured pick-up coil voltage profiles, $V(t)$.

For the stand-alone jump coils, the field profiles obtained with the pick-up coil agree well with the current profiles. However, when the Helmholtz coil is mounted at the EPR probehead and the pick-up coil is installed inside the slotted brass ENDOR cavity at the sample position the additional transient-field component is detected. It is opposing the coil-generated field while it rises, and it is supporting the coil field while it falls (see Fig. 5b). This field component develops right after the coil field is stepped on and off, reaches a maximum of $0.3\Delta B$ in about 50 ns and then decays with a characteristic time constant of about 1 μ s. When measured in the same configuration but without ENDOR cavity, the 1 μ s component disappears and another transient-field component becomes detectable, which has a decay time of about 7 μ s and a peak amplitude of $0.06\Delta B$. These additional fields are obviously generated by eddy currents. The fast component can be ascribed to currents within the cavity walls, which are still not completely slotted (for the sake of mechanical stability one side of the cavity attached to the coupling waveguide is not slotted). The slow (and weaker) component is generated by induced eddy currents in conductive elements surrounding the cavity.

Measurements with the pick-up coil performed at different setup configurations allowed us to separate and assign different eddy-field components. These measurements, however, give no information on the field homogeneity over the typical EPR sample volume, which is much smaller than the volume of the pick-up coil. Moreover, the accuracy of this technique to measure the slow transient fields is not sufficient. Fortunately, the pulsed EPR signals themselves provide the desired information and allow exact measurements of the transient magnetic fields.

4.3 FID EPR Measurements

A LiF:Li sample was used for measuring the field-jump characteristics by EPR. The EPR signal of this sample originates from conduction electrons in nanometer particles of disperse metallic lithium in a neutron-irradiated LiF crystal [24]. The small LiF:Li sample (crystal of 0.5 by 0.2 by 0.03 mm) gives a very intense signal: The free-induction decay (FID) signal, with a decay-time constant of about 200 ns, can be detected free of noise even after a microsecond delay, and even when the FID was excited at a resonance offset of several tens of Gauss, i.e., under small-angle excitation conditions. This makes the LiF:Li sample very attractive for testing and calibrating field-jump devices.

Figure 6a shows FID traces generated by a sequence of 18 ns microwave pulses that were applied at different times during a field jump of 4200 ns duration and 25 G amplitude, as estimated from current measurements. The static magnetic field B_0 was set 40 G below EPR resonance, and the field jump was added to B_0 to reduce the negative resonance offset. The off-resonance frequency shifts were obtained by Fourier transforming the FID traces. In Fig. 6b these fre-

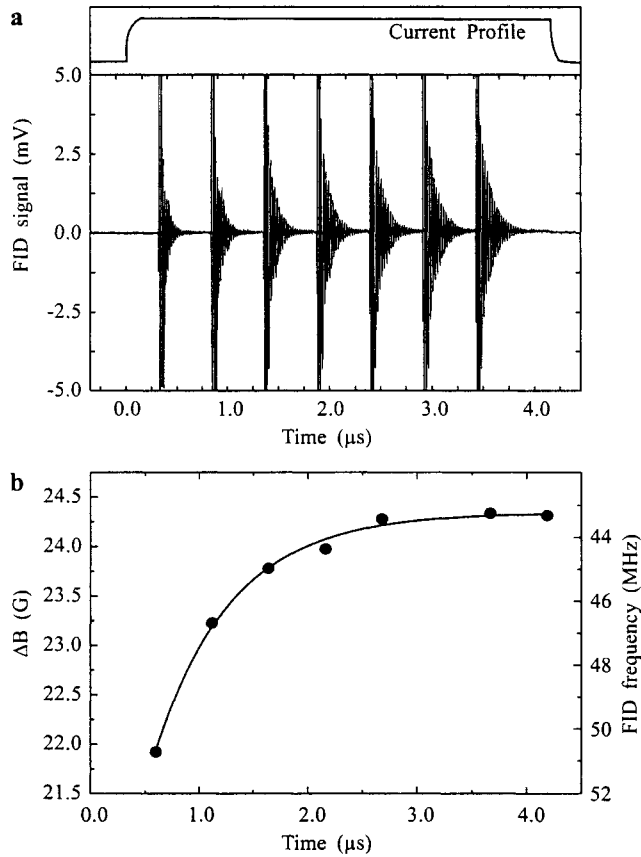


Fig. 6. **a** Multiple FID decays detected during a field-jump pulse of 4.2 μs duration to determine the jump-field time profile. **b** Magnetic-field amplitude (FID frequency) during the jump pulse vs. time. The point size reflects the error in FID-frequency determination by Fourier transformation of the echo decays.

quencies are plotted vs. time delay after the current was switched on. Reduction of the FID frequency indicates an increase of the effective field jump, which approaches the coil-determined value after the eddy currents have disappeared. The analysis of the field vs. time profiles results in the following estimates: The eddy-field amplitude, B_{ed} , reaches its maximum of $0.3\Delta B$ at the end of the switching-on period of the external field (approximately in 50 ns). The subsequent decay of the eddy field occurs, to a good approximation, biexponentially:

$$B(t) \approx -0.3\Delta B[C_1 \exp(-t/\tau_{\text{ed1}}) + C_2 \exp(-t/\tau_{\text{ed2}})], \quad (2)$$

where the negative sign indicates the eddy-field direction being opposite to the stepped field. The relative amplitudes are $C_1 = 0.8$ and $C_2 = 0.2$. The decay-time constants are $t_{\text{ed1}} = 0.9 \pm 0.1 \mu\text{s}$ and $t_{\text{ed2}} = 6 \pm 1 \mu\text{s}$. These numbers are in reason-

able agreement with those determined by the pick-up coil measurements, where the fast component was referred to the eddy currents in the slotted cavity.

The behavior of the transient eddy field after the field jump was examined by a sequence of FID traces in the same way as described above. The time characteristics of the field induced by the turn-off eddy currents were found to be close to those determined for the turn-on induction. Measured amplitudes of both fast and slow field components were affected by superposition with the oppositely directed fields generated by the turn-on process, in accordance with the expression:

$$B(t) \approx 0.3\Delta B[C_1(1 - \exp(-T_p/\tau_{ed1}))\exp(-t/\tau_{ed1}) + C_2(1 - \exp(-T_p/\tau_{ed2}))\exp(-t/\tau_{ed2})]. \quad (3)$$

Here T_p stands for the duration of the current pulse within the Helmholtz coil (not to be confused with the total field-pulse length, t_{fp} , introduced in Sect. 2). Thus, to reduce the amplitudes of these residual components, a submicrosecond T_p is required. Although such fast current pulses through the Helmholtz coils can be generated with the present device, certain limitations prevent us from using the shortest T_p : according to Eq. (2), the drift of the stepped field for the 160 G jump amplitude diminishes to the required level of $(d\Delta B/dt) < 4 \text{ G}/\mu\text{s}$ (see Sect. 2, requirement 2) only at 2 ms after the jump had been started. Therefore, for a field-jump amplitude of 160 G the driving current pulse duration T_p cannot be reduced below this limit, and the slow residual field component of about 3 G amplitude affects echo responses long after the jump.

As for the spatial homogeneity of the field jump, its significant distortion is manifested by an accelerated decay of the FID signals (see Fig. 6a): the evaluated inhomogeneity of eddy field over the sample volume reaches 10% of the field amplitude for the slow component, and 20% of the field amplitude for the fast component. Thus, in 2 μs after the 160 G field jump had been switched on, the field inhomogeneity equals 1.6 G, and in 2 μs after this jump inhomogeneity equals 0.95 G.

The drift, inhomogeneity and residual-amplitude values of the jump field are proportional to the amplitude of the jump. Our measurements with the slotted brass ENDOR cavity show that these quantities become unacceptably large at jump amplitudes sufficiently large for high-field FJ-PELDOR on nitroxides. Thus, further development of the brass probehead was required to reduce the transient eddy field or to make it decay faster. Below we describe the modification of the probehead which allows for considerable reduction of the transient shielding field.

5 Reduction of the Transient Shielding of the Field Jump

5.1 High-Resistance EPR Cavity to Diminish Eddy Currents

The straightforward way to suppress eddy currents in the probehead is to replace its conductive elements by those manufactured from insulating materials (e.g., ce-

ramics). However, since the cavity walls and coupling elements must support mw currents, they should, if made from insulator, be surface-plated by a thin conductive film. Machining miniature W-band cavities from ceramics with subsequent polishing and metal plating encounters severe problems due to the brittleness of ceramics and the different thermal properties of ceramic and metallic elements in contact. Consequently, we considered a highly resistive metallic alloy as the cavity material, alternative to ceramics. As expected, this substitution of highly conductive metal by highly resistive alloy with thin gold plating leads to considerable shortening of unwanted transient processes screening the field jump.

An exact copy of the slotted brass ENDOR cylindrical TE_{011} cavity was manufactured from Ti-6Al-4V alloy. Compared to brass, this alloy has a 25 times higher resistivity and a 4 times smaller temperature-resistance coefficient [25, 26]; Ti-6Al-4V: electrical resistivity, $168 \text{ m}\Omega \cdot \text{cm}$; temperature coefficient, 0.0004

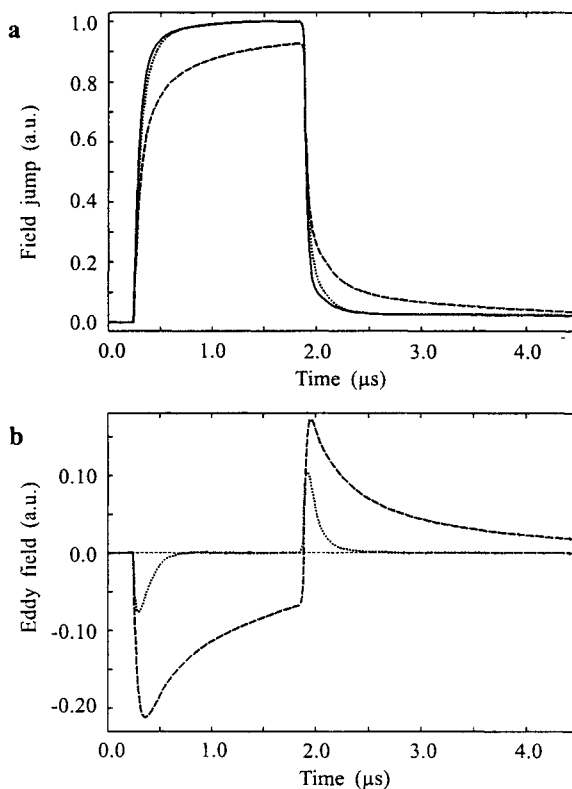


Fig. 7. **a** Time profiles of the field jump obtained by numerical integration of the pick-up coil voltage profiles for a 100 G, $1.6 \mu\text{s}$ jump: solid line, jump coils mounted on the probehead without cavity; dashed line, jump coils mounted on the probehead with slotted brass cavity; dotted line, jump coils mounted on the probehead with slotted high-resistance Ti-6Al-4V cavity. **b** Profiles of the transient magnetic fields generated by eddy currents in the slotted brass cavity (dashed line) and in the slotted Ti-6Al-4V cavity (dotted line). They are obtained from the profiles in **a** by subtracting the solid curve from the respective dashed and dotted curves.

K^{-1} ; brass 70Cu-30Zn: electrical resistivity, $6.1 \text{ m}\Omega \cdot \text{cm}$; temperature coefficient, 0.0014 K^{-1} .

For comparison, the corresponding resistivity data for B_4C and SiC ceramics are $1\text{--}10 \text{ W} \cdot \text{cm}$ and $10^3\text{--}10^5 \text{ }\Omega \cdot \text{cm}$, respectively. For a sufficiently high Q value ($Q = 2000$), the inner surface of the cavity was gold-plated (about 4 mm). Consequently, no loss of EPR sensitivity and of mw field amplitude was found for this cavity as compared to the prototype brass cavity.

The reactive fields in the Ti-6Al-4V probehead were determined from pick-up coil measurements and FID frequency evaluations similar to those described above for the prototype brass cavity. Figure 7a shows representative field-time profiles for a 100 G, 1.6 μs jump at three configurations: jump coils mounted on the probehead without cavity, jump coils mounted on the probehead with the brass ENDOR cavity, and with the Ti-6Al-4V cavity. The screening field from eddy currents in the cavity (the fast component in our previous consideration) was found to decay in the Ti-6Al-4V cavity with a time constant of $110 \pm 10 \text{ ns}$. This is an order of magnitude faster than that in the brass cavity of the same geometry.

The eddy-field amplitude at 500 ns after the turn-on field step is $3 \cdot 10^{-3} \cdot \Delta B_1$, which, for a 160 G field jump, corresponds to 0.5 G. Thus, to satisfy the requirements for FJ-PELDOR experiments (to achieve a stable peak-field value and to avoid residual fields after switching off) with the Ti-6Al-4V cavity, a duration of the field jump of about 700 ns and an after-pulse delay of 500 ns are estimated, which determine a minimum stimulated-echo time T of 1.2 μs . This pulse pattern would already allow precession-frequency transfer experiments on nitroxide radical pairs in high magnetic fields to be made for the determination of the nanometer distance and orientation of spin labels in disordered samples.

5.2 Compensation of Eddy Fields by Shimming Eddy-Current Loops

For further reduction of transient eddy fields, one should revise not only the EPR cavity but also other elements of the probehead. To avoid this rather elaborate intrusion into the W-band probehead, we have tried a novel technical solution: the passive shimming of transient eddy fields. Passive correction of stationary magnetic fields by specially shaped magnetic inserts (shims) is known since times. In analogy to this technique, correction of transient eddy fields within a small volume, where the sample is located, can be achieved by insertion of small conductive loops close to the sample. According to a ring model for circular eddy currents, a loop position can be found where its circular current, induced by an external field step, creates a transient field at the sample which is opposite in direction to the "intrinsic" eddy field, created by currents within the probehead. To fit amplitude and time profile of this correction field for compensating the unwanted eddy field, at least in a certain time interval, size, resistance and location of the loop have to be carefully adjusted. If such an adjustment is achieved for a certain amplitude of the field step, it will inherently be valid also for any

other step amplitude. Another aspect of the adjustment has to be considered: at different temperatures of the EPR experiment the loop and the probehead resistances change. This modifies the compensation field and the "intrinsic" eddy fields. To account for this effect, the loop material has to be properly chosen to fit the temperature-resistance behavior of the probehead.

In our preliminary experiments with shimming eddy-current loops we managed to suppress eddy-field screening by more than an order of magnitude, in a time interval of several microseconds just after the field step. Moreover, even a small eddy-field gradient at the sample was largely compensated by proper asymmetric shift of the loops with respect to the sample. Further development of this promising technique of passive shimming of eddy fields is in progress.

6 Signal Distortions Caused by the Field Jump

Lorentz forces acting on the Helmholtz coils in the strong B_0 field during the current pulse are directed radially and, thus, mostly compensate each other. Nevertheless, we found it necessary to install the coils mechanically well-isolated from the microwave cavity and from its coupling and tuning parts in the EPR probehead. As a result, effects of mechanical distortions ("microphonics") on the detected signal became negligible. On the other hand, the strong current and high-voltage pulses induce considerable electromagnetic stray-field irradiation. This affects the sensitive receiver circuit of the EPR spectrometer and creates a spurious signal in the detection channel. Even after shielding procedures for these detection circuits, the spurious signal still has an amplitude comparable to that of the echo signal of nitroxide samples. It decays in about a microsecond and overlaps with the echo signal causing severe problems with data acquisition and analysis. Fortunately, this spurious signal was found to be highly reproducible and, after separate accumulation at off-resonance position, can be subtracted from the mixture of echo and distortion signals. This data processing reduces contributions of the spurious signal to the noise level.

7 Conclusions

The present results show that submicrosecond magnetic-field pulses, added to the Zeeman field, can be generated and handled in W-band high-field EPR spectroscopy. They satisfy the requirements of FJ-PELDOR on pairs of nitroxide spin labels, provided highly resistive alloys are used as an EPR cavity material. FJ-PELDOR experiments pose stringent requirements on the field-jump device because the reactive field of eddy currents, induced by the field jump within the conductive parts of the probehead, superimposes with the source field and distorts the field-time profile and field homogeneity. Further reduction of these distortions can be achieved by consequent replacement of conductive parts of the probehead by insulating parts. Additional improvement is achieved by introduc-

ing special shimming loops that passively create transient fields to compensate the unwanted eddy fields.

The developed field-jump technique at high Zeeman field and mw frequency (W-band) was designed for orientation-resolving dipolar spectroscopy of paired nitroxide radicals in disordered frozen samples. Because of high orientation selectivity in W-band high-field EPR, this method promises to provide quasi-discrete spectra of dipolar-interaction frequencies for radical pairs with a particular orientation selected from other orientations in the disordered solid. Frequency information contained in such discrete spectra, as compared to that of spectra provided by dipolar spectroscopy with nonselective pulses, is less affected by distortions caused by experimental imperfections (limited excitation bandwidth, finite dead time, etc.). The dipolar-frequency value depends on two factors: the distance between the paired radicals and the orientation of the pair axis with respect to the external magnetic-field direction. The orientational factor can be monitored by changing the spectral positions selected for FJ-PELDOR measurements across the anisotropic spectrum of the nitroxide radicals. This magneto-selection is improved in high-field EPR. Analysis of angular characteristics of pair geometry on the basis of these measurements requires, however, the distance factor to be determined independently. The distance information can be provided, for example, by nonselective pulse dipolar spectroscopy [9] operating at lower mw frequency, i.e., by pulsed X-band EPR. Thus, we conclude that the proper strategy for studying both angular and distance characteristics of radical pairs appears to be a multifrequency pulsed dipolar spectroscopy.

Work is in progress in the Berlin laboratory to use the described field-jump device in pulsed W-band EPR for studying the geometry of pairs of nitroxide side chains in site-specifically spin-labeled double mutants of protein systems.

Acknowledgements

This work was supported by the Deutsche Forschungsgemeinschaft (Schwerpunktprogramm SPP 1051, Sonderforschungsbereich SFB 498) and by the Russian Foundation of Basic Research (RFBR 99-03-33252a) which are gratefully acknowledged.

References

1. Schweiger A., Jeschke G.: Principles of Pulse Electron Paramagnetic Resonance. Oxford: Oxford University Press 2001.
2. Borbat P.P., Costa-Filho A.J., Earle K.A., Moscicki J.K., Freed J.H.: *Science* **291**, 266–269 (2001)
3. Berliner L.J., Eaton G.R., Eaton S.S. (eds.): Distance Measurements in Biological Systems by EPR (Biological Magnetic Resonance, vol. 19). New York: Plenum 2000.
4. Hustedt E.J., Beth A.H.: *Annu. Rev. Biophys. Biomol. Struct.* **2**, 129–153 (1999)
5. Berliner L.J. (ed.): Spin Labeling: The Next Millennium (Biological Magnetic Resonance, vol. 14). New York: Plenum 1998.
6. Rabenstein M.D., Shin Y.-K.: *Proc. Natl. Acad. Sci. USA* **92**, 8239–8243 (1995)

7. Steinhoff H.-J., Radzwill N., Thevis W., Lenz V., Brandenburg D., Antson A., Dodson G., Wollmer A.: *Biophys. J.* **73**, 3287–3298 (1997)
8. Lebedev Ya.S.: *Appl. Magn. Reson.* **7**, 339–362 (1994)
9. Jeschke G., Pannier M., Godt A., Spiess H.W.: *Chem. Phys. Lett.* **331**, 243–252 (2000)
10. Milov A.D., Maryasov A.G., Tsvetkov Y.D.: *Appl. Magn. Reson.* **15**, 107–143 (1998)
11. Pannier M., Veit S., Godt A., Jeschke G., Spiess H.W.: *J. Magn. Reson.* **142**, 331–340 (2000)
12. Larsen R.G., Singel D.J.: *J. Phys. Chem.* **98**, 5134–5146 (1993)
13. Rangan S.K., Bhagat V.R., Sastry V.S.S., Venkataraman B.: *J. Magn. Reson.* **33**, 227–240 (1979)
14. Dzuba S.F., Maryasov A.G., Salikhov K.M., Tsvetkov Yu.D.: *J. Magn. Reson.* **58**, 95–117 (1984)
15. Dubinskii A.A., Maresch G.G., Spiess H.W.: *J. Chem. Phys.* **100**, 2437–2448 (1994)
16. Hornak J.P., Freed J.H.: *Chem. Phys. Lett.* **101**, 115–119 (1983)
17. Piasecki W., Froncisz W., Hyde J.S.: *Rev. Sci. Instrum.* **67**, 1896–1904 (1996)
18. Rinard G.A., Quine R.W., Ghim B.T., Eaton S.S., Eaton R.R.: *J. Magn. Reson. A* **122**, 50–57 (1996)
19. Avdievich N.I., Gerfen G.J.: *J. Magn. Reson.* **153**, 178–185 (2001)
20. Nesselov Y.E., Surek J.T., Thomas D.D.: *J. Magn. Reson.* **153**, 7–14 (2001)
21. Saalmueller J.W., Long H.W., Maresch G.G., Spiess H.W.: *J. Magn. Reson. A* **117**, 193–208 (1995)
22. Willer M., Granwehr J., Forrer J., Schweiger A.: *J. Magn. Reson.* **133**, 46–52 (1998)
23. Burghaus O., Rohrer M., Götzinger T., Plato M., Möbius K.: *Meas. Sci. Technol.* **3**, 765–774 (1992)
24. Kaplan R., Bray P.J.: *Phys. Rev.* **129**, 1919–1935 (1963)
25. Tai C.-C., Rose J.H., Moulder J.C.: *Rev. Sci. Instrum.* **67**, 3965–3972 (1996)
26. Lide D.R. (ed.): *CRC Handbook of Chemistry and Physics*, pp. 12–44. New York: CRC Press 1996.

Authors' address: Anton N. Savitsky, Freie Universität Berlin, Institut für Experimentalphysik, Amim-allee 14, 14195 Berlin, Germany